

Dual Neutral Sphingomyelinase-2/Acetylcholinesterase Inhibitors for the treatment of Alzheimer's disease

Tina Bilousova, Bryan J. Simmons, Rachel R. Knapp, Chris J. Elias, Jesus Campagna, Mikhail Melnik, Sujyoti Chandra, Samantha Focht, Chunni Zhu, Kanagasabai Vadivel, Barbara Jagodzinska, Whitaker Cohn, Patricia Spilman, Karen H. Gylys, Neil K. Garg, and Varghese John

ACS Chem. Biol., **Just Accepted Manuscript** • Publication Date (Web): 30 Apr 2020

Downloaded from pubs.acs.org on May 1, 2020

Just Accepted

"Just Accepted" manuscripts have been peer-reviewed and accepted for publication. They are posted online prior to technical editing, formatting for publication and author proofing. The American Chemical Society provides "Just Accepted" as a service to the research community to expedite the dissemination of scientific material as soon as possible after acceptance. "Just Accepted" manuscripts appear in full in PDF format accompanied by an HTML abstract. "Just Accepted" manuscripts have been fully peer reviewed, but should not be considered the official version of record. They are citable by the Digital Object Identifier (DOI®). "Just Accepted" is an optional service offered to authors. Therefore, the "Just Accepted" Web site may not include all articles that will be published in the journal. After a manuscript is technically edited and formatted, it will be removed from the "Just Accepted" Web site and published as an ASAP article. Note that technical editing may introduce minor changes to the manuscript text and/or graphics which could affect content, and all legal disclaimers and ethical guidelines that apply to the journal pertain. ACS cannot be held responsible for errors or consequences arising from the use of information contained in these "Just Accepted" manuscripts.

1
2
3 **Dual Neutral Sphingomyelinase-2/Acetylcholinesterase Inhibitors for the**
4 **Treatment of Alzheimer's disease**
5
6
7

8
9 Tina Bilousova^{1,3}, Bryan J. Simmons², Rachel R. Knapp², Chris J. Elias¹, Jesus
10 Campagna¹, Mikhail Melnik³, Sujyoti Chandra¹, Samantha Focht¹, Chunni Zhu¹,
11 Kanagasabai Vadivel¹, Barbara Jagodzinska¹, Whitaker Cohn¹, Patricia Spilman¹,
12 Karen H. Gyllys³, Neil K. Garg^{2*}, Varghese John^{1*}
13
14
15

16
17 *¹Drug Discovery Laboratory, Department of Neurology, Mary S. Easton Center for*
18 *Alzheimer's Disease Research, University of California, Los Angeles, CA 90095, United*
19 *States*
20
21

22 *²Department of Chemistry and Biochemistry, University of California, Los Angeles, CA*
23 *90095, United States*
24
25

26 *³School of Nursing, University of California, Los Angeles, CA 90095, United States*
27
28

29 **Corresponding authors*
30
31

32 **ABSTRACT**
33

34 We report the discovery of a novel class of compounds that function as dual inhibitors of
35 the enzymes neutral sphingomyelinase-2 (nSMase2) and acetylcholinesterase (AChE).
36 Inhibition of these enzymes provides a unique strategy to suppress the propagation of
37 tau pathology in treatment of Alzheimer's disease (AD). We describe the key SAR
38 elements that affect relative nSMase2 and/or AChE inhibitor effects and potency, in
39 addition to the identification of two analogs that suppress the release of tau-bearing
40 exosomes in vitro and in vivo. Identification of these novel dual nSMase2/AChE
41 inhibitors represents a new therapeutic approach to AD and has the potential to lead to
42 the development of truly disease-modifying therapeutics.
43
44
45
46
47
48
49
50
51
52
53
54
55
56
57
58
59
60

INTRODUCTION

Alzheimer's disease (AD) is the most prevalent age-related neurodegenerative disorder and, currently, there are no effective disease-modifying therapies available for the treatment of AD. The number of AD cases in the US is ~5.8 million patients and this number is expected to rise to 50 million by 2050. The estimated global socioeconomic costs of AD and related dementias are predicted to reach \$2 trillion by the year 2030.¹

AD brain tissue is characterized by the presence of senile plaques composed mainly of aggregated amyloid- β peptide (A β), neurofibrillary tangles (NFTs) composed of pathological forms of the microtubule-stabilizing protein tau, chronic neuroinflammation, and loss of neurons.² Clinically, it is thought that the underlying mechanisms of disease are initiated as early as 20 years before the onset of signs and symptoms. During this asymptomatic period, proteopathic proteins are believed to accumulate, leading to structural alterations and the neuronal dysfunction and loss that leads frequently to Mild Cognitive impairment (MCI). MCI then progresses to full-blown AD-related memory deficits, decline of other cognitive skills, and in advanced AD, the inability to participate in activities of daily living.³

While the exact mechanisms of disease progression have not been fully elucidated, it is thought that increased A β production at the synapse and/or impaired clearance, results in synaptic loss. Contemporaneously and in conjunction with A β accumulation, there is hyperphosphorylation and oligomerization of tau that eventually leads to neuronal toxicity, NFT formation, and neuronal cell death. Diseased neurons can release these toxic phosphorylated forms of tau (p-tau) in proteopathic seeds, which can then be taken up by surrounding or interconnected neurons, leading to templating and propagation of the pathological aggregates in prion-like fashion. The propagation of the disease follows a spatiotemporal pattern with A β plaques first appearing in the basal forebrain, then the frontal, temporal and occipital lobes of the cortex. NFTs form in the locus coeruleus and in the allocortex of the medial temporal lobe.⁴ Both A β and tau pathologies spread through the brain during disease progression.²

Given the importance of tau, significant attention is now being paid to the mechanisms of pathological tau spread in AD with the goal of identifying targets for novel therapies to prevent disease progression.⁵ Historically, A β pathology has been

1
2
3 thought to be causative in AD,⁶⁻⁷ but multiple clinicopathological evaluations, as well as
4 recent in vivo imaging studies, suggest that the cognitive status of AD patients
5 correlates most closely with region-specific brain atrophy and distribution of the hyper-
6 phosphorylated and aggregated pathological forms of tau that lead to the formation of
7 NFTs.⁸⁻¹¹ Longitudinal studies have confirmed that propagation of tau pathology
8 correlates significantly with cognitive decline.¹²⁻¹³ These data suggest that suppression
9 of propagation of tau pathology in AD may have a disease-modifying effect.

15 Prompted by the findings described above, we undertook a screening effort to
16 identify inhibitors of tau propagation. As will be discussed below, this led to the
17 discovery of dual inhibitors of two enzymes: neutral sphingomyelinase 2 (nSMase2)
18 and acetylcholine esterase (AChE), a key enzyme implicated in AD. In our in vitro
19 studies, the identified dual inhibitors prevented the spreading of tau in cell culture
20 systems using assays we have previously reported.¹⁴

25 NSMase2 is an enzyme responsible for hydrolysis of sphingomyelin to
26 ceramide/phosphatidylcholine and has been implicated in the spread of AD pathology.
27 Pharmacological inhibition or genetic depletion of nSMase2 has been shown to
28 suppress progression of both A β and tau pathology in animal models.¹⁵⁻¹⁷ nSMase2
29 activity plays an important role for normal brain function, but its activity increases with
30 age leading to dysregulation in sphingomyelin turnover.¹⁸⁻²² There is over-activation of
31 nSMase2 in AD, and brain ceramide levels have been found to be elevated in AD
32 patient cerebrospinal fluid (CSF), compared to age-matched control subjects.²³ The
33 ceramide/sphingomyelin imbalance is greater in individuals that express apolipoprotein
34 E4 (ApoE4), the major genetic risk factor for sporadic, late onset AD.²⁴ NSMase2 is a
35 key enzyme involved in biogenesis of brain exosomes through the Endosomal Sorting
36 Complex Required for Transportation (ESCRT)-independent pathway.²⁵ Brain
37 exosomes are a type of extracellular vesicle (EV), that are 40-150 nm in diameter and
38 are released by brain cells when multivesicular endosomes fuse with the plasma
39 membrane.²⁵⁻²⁶ They are involved in normal brain function, but a subset produced by
40 the ESCRT-independent pathway involving nSMase2 have been shown to carry
41 disease-propagating proteopathic seeds, such as tau oligomers, in AD.^{14-15, 17, 27} Tau
42 oligomers have been found to be associated with neuronal exosomes in both cell
43
44
45
46
47
48
49
50
51
52
53
54
55
56
57
58
59
60

1
2
3 culture medium and transgenic AD/tauopathy model brain tissue, as well as in AD
4 patient plasma and CSF.^{15, 28-33}

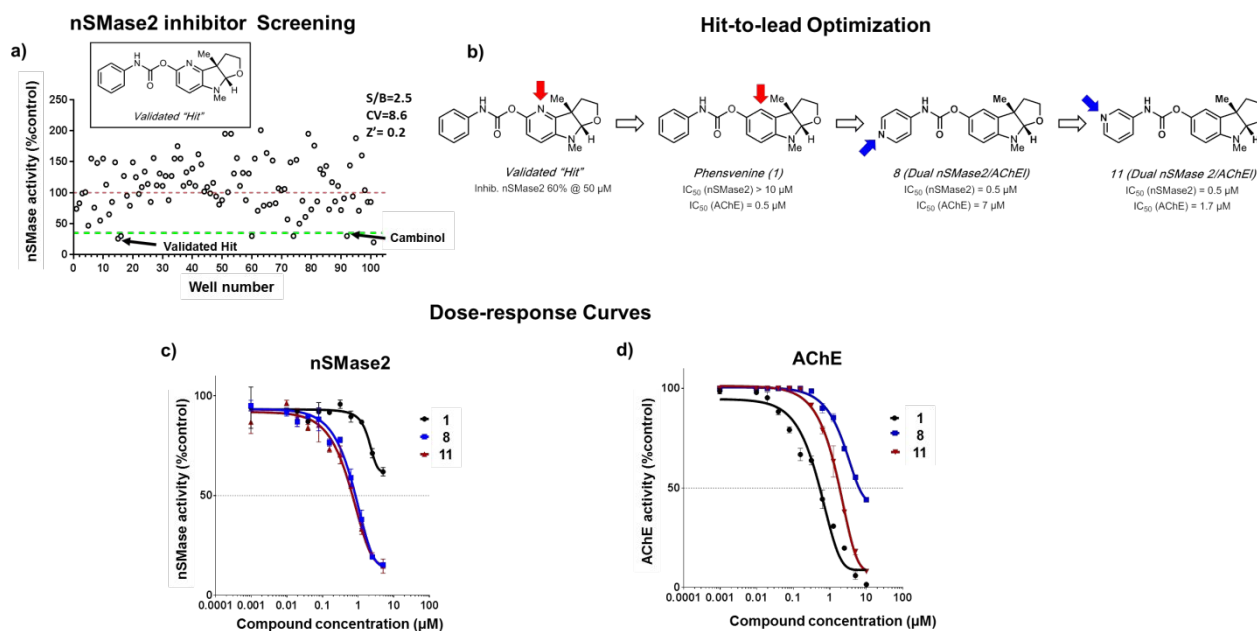
5
6 Despite recent progress, the current armamentarium of nSMase2 inhibitors have
7 poor drug-like properties and oral brain permeability.³⁴⁻³⁵ Thus, our initial goal was to
8 identify nSMase2 inhibitors that overcome these limitations for the development of
9 preclinical candidates for AD. Using an nSMase2 inhibitor screening assay, we
10 identified a novel furoindoline compound 'validated hit'. Further structural alterations of
11 this initial hit generated compounds that resulted in the identification of novel dual
12 inhibitor analogs that not only inhibit nSMase2 activity, but also inhibit
13 acetylcholinesterase (AChE) enzyme activity and suppress p-tau propagation.
14
15
16
17
18
19

20 AChE inhibitors (AChEIs) are currently one of only two classes of FDA-approved AD
21 therapeutics; they have demonstrated amelioration of symptoms in AD, being most
22 effective in mild and moderate AD.³⁶ Inhibition of AChE leads to increased levels of
23 acetylcholine (ACh) at the synapse and in brain parenchyma, and provides support for
24 cholinergic synaptic plasticity even during progressive loss of cholinergic innervation
25 from the basal forebrain.³⁷ However, AChEI's treatment only provides short term
26 benefits in AD and does not block the progression of the disease.
27
28
29
30
31

32 The dual nSMase2/AChE inhibitors we describe herein represent a new therapeutic
33 paradigm enabling target engagement by a single agent of two enzymes in the brain
34 that play a role in spread of tau pathology.³⁸ This promising approach could lead to an
35 effective treatment for AD. These agents have the potential to be disease-modifying by
36 suppressing disease progression through exosome-mediated tau propagation, while
37 also providing symptomatic relief through support of ACh-mediated cognitive
38 enhancement. Interestingly, in mild to moderate AD, there is significantly decreased
39 cholinergic activity and high levels of p-tau in CSF-derived exosomes, thus treating
40 patients in these stages of the disease with dual nSMase2/AChE inhibitors could be
41 highly beneficial.³³ We propose a mechanism of action for these dual inhibitors
42 involving nSMase2 mediated suppression of tau oligomer release in brain exosomes by
43 presynaptic neurons, increased ACh levels at the synapse through AChE inhibition,
44 along with the suppression of tau oligomer uptake through ACh receptors by
45 postsynaptic neurons.³⁸
46
47
48
49
50
51
52
53
54
55
56
57
58
59
60

RESULTS AND DISCUSSION

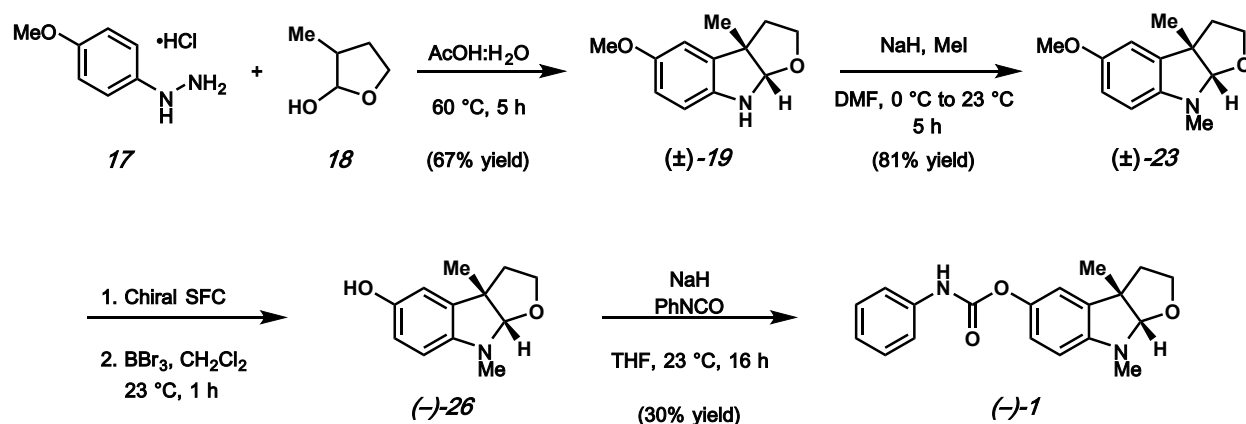
Screening for and optimization of selective nSMase2 and dual nSMase2/AChE inhibitors. We initiated the present study by screening a small molecule compound library for effects on nSMase2 activity. The ~70 compound library were mostly fused indolines we had prepared previously through interrupted Fischer indolization methodology that have structural resemblance to phenserine and known AChE inhibitors. Using an Amplex Red neutral sphingomyelinase enzyme activity assay several hits were identified that inhibited $\geq 60\%$ nSMase2 activity at a concentration of 50 μM , as shown in the scatterplot (**Figure 1a**). The known nSMase2 inhibitor cambinol¹⁴ was used as a positive control for the screening assay. After retesting, one hit (**Figure 1a**) was validated at 50 μM and selected for further hit-to-lead optimization.



1
2
3 **Figure 1.** Screening and identification of novel dual nSMase2/AChE inhibitors: a) nSMase2 inhibitor screening using Amplex Red-coupled assay revealed several hits that inhibited activity $\geq 60\%$; b) hit-to-lead optimization of the validated hit shows removal of the nitrogen group from the furoindoline aryl ring (red arrow) and addition of nitrogen to the carbamate phenyl ring at either the 3 or 4 positions (blue arrow) results in enhanced potency for nSMase2 inhibition and varied AChE inhibition; c) Dose-response analysis for compounds **1**, **8**, and **11** in the nSMase2 assay; and d) Dose-response analysis for compounds **1**, **8**, and **11** in the AChE assay.

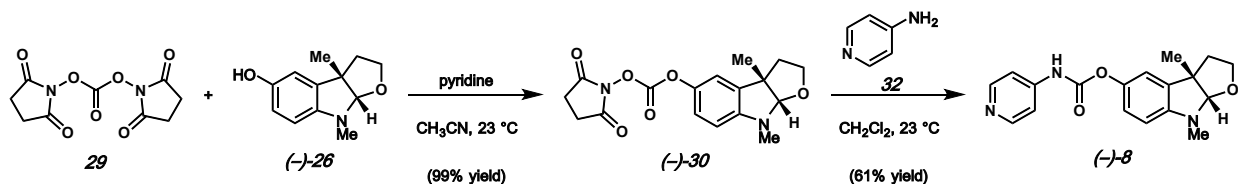
13 Optimization efforts led to the synthesis and evaluation of analogs. Our synthetic approach to the validated hit and analogs will be described subsequently, but a summary of our optimization effort leading to key dual inhibitor analogs **8** and **11** is shown in **Figure 1b**. Given the structural similarity between the validated hit and known AChE inhibitor phensvenine (**1**) we initially prepared this analog to check if it was also an nSMase2 inhibitor. Dose-response analysis revealed that phensvenine (**1**) indeed has nSMase2 inhibitory activity (**Figure 1c**) but is a more potent inhibitor of AChE with an $IC_{50} = 0.5 \mu M$ (**Figure 1d**). In contrast, the dual inhibitors **8** and **11** were more potent nSMase2 inhibitors ($IC_{50} = 0.5 \mu M$) with varying AChE inhibitory activity (**Figure 1c & 1d**). Interestingly, replacement of the oxygen in the furoindoline ring of phensvenine (O \rightarrow N-CH₃), as seen in phenserine a known potent AChE inhibitor, results in the loss of any detectable nSMase2 inhibitory activity ($IC_{50} > 50 \mu M$). Posiphen, the (+)-enantiomer of phenserine, is reported to be a weak AChE inhibitor and did not show detectable nSMase2 inhibitor activity ($IC_{50} > 50 \mu M$).³⁹ We therefore focused on the (-)-enantiomer for the dual inhibitor optimization effort.

39 The synthesis of the validated hit and analogs were made possible by using the interrupted Fischer indolization reaction and variants thereof.⁴⁰ As an example, the interrupted Fischer indolization route to (-)-phensvenine (**1**) is shown in Scheme 1. Treatment of aryl hydrazine **17** and lactol **18** with acetic acid furnished furoindoline **19** in 67% yield. Subsequent *N*-methylation provided **23**. At this stage, the enantiomers could be resolved using chiral SFC. As depicted for the (-)-enantiomer, *O*-deprotection was achieved using BBr₃, thus furnishing (-)-**26**. Lastly, treatment with NaH and phenylisocyanate furnished (-)-phensvenine (**1**). It should be noted that (-)-enantiomers were specifically targeted given the known stereospecificity of phenserine for AChE inhibition.^{39, 41}



Scheme 1. Synthesis of (-)-phensvenine (**1**)

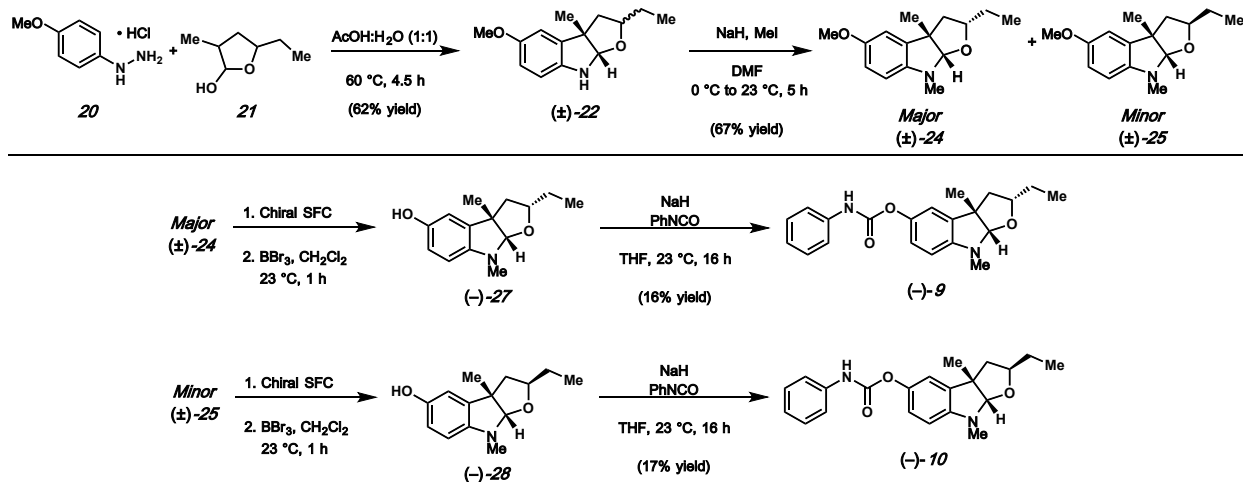
The synthetic route was readily amenable to the synthesis of analogs, particularly by exploiting intermediate (-)-**26** as a means to access different carbamate substitution patterns. Scheme 2 provides an example, in the context of the synthesis of analog (-)-**8**. Alcohol (-)-**26** readily underwent reaction with **29** to furnish carbonate (-)-**30**. Upon treatment with 4-aminopyridine (**32**), (-)-**8** was obtained in 61% yield. The syntheses of other carbamate analogs are provided in the SI.



Scheme 2. Synthesis of furoindoline analog (-)-**8**

Scheme 3 shows the routes used to prepare two analogs bearing substitution on the furoindoline ring. Interrupted Fischer indolization using hydrazine **20** and lactol **21** proceeded smoothly to give **22** as a mixture of diastereomers in racemic form. Upon methylation, diastereomers **24** and **25** were accessed and could be separated by silica gel chromatography. Each diastereomer was then elaborated through a sequence

involve separation by chiral SFC, demethylation, and carbamate formation. This unoptimized synthetic sequence delivered (–)-**9** and (–)-**10**, respectively for initial biological evaluation.



Scheme 3. Synthesis of furoindoline analogs (–)-**9** and (–)-**10**

In total, sixteen analogs were prepared as part of the optimization efforts. The structures of these analogs, dose-response analysis results, predicted brain permeability data, and binding efficiency to human serum albumin (HSA) are shown in Table 1. Our SAR analysis reveals structural elements in this series required for enhanced nSMase2 and/or AChE inhibition. Substitutions in the carbamate phenyl ring pointed to a critical role for positions 3 and 4 as key control elements for nSMase2 and/or AChE inhibition. Substitution in the 4-position leads to increased selectivity for nSMase2 inhibition (such as for compounds **2**, **4** and **8**). In contrast, substitution in the 3-position leads to increased selectivity for AChE inhibition (such as **3** and **11**). Introduction of electron donating groups (**3**, **6**, and **7**) at position 3 increased potency of AChE inhibition, while an electron withdrawing group (such as in **14**) resulted in decreased potency. Importantly, replacement of the phenyl ring with a pyridyl ring in the carbamate moiety generally decreased potency of AChE inhibition and markedly enhanced potency for nSMase2 inhibition (e.g. **8**, **11**, **12**). Most of the analogs (except **4**) showed high predicted brain permeability by *in silico* StarDrop analysis and in a parallel artificial membrane permeability assay (PAMPA). A low degree of binding to

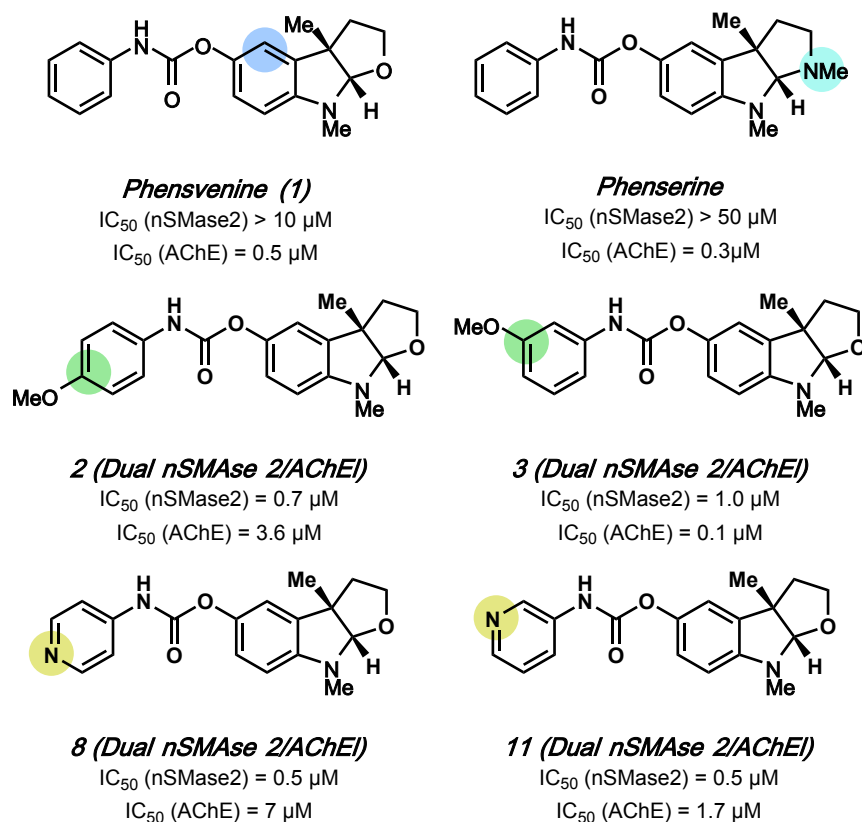
1
2
3 human serum albumin (HSA) measured for most of the compounds, especially **8**, **11**,
4 **12**, and **13**.
5
6
7

8 **Table 1.** Structure and characteristics of carbamate furoindoline analogs.
9
10
11
12
13
14
15
16
17
18
19
20
21
22
23
24
25
26
27
28
29
30
31
32
33
34
35
36
37
38
39
40
41
42
43
44
45
46
47
48
49
50
51
52
53
54
55
56
57
58
59
60

Compound #	Structure	MW (g/mol)	IC ₅₀ nSMase2 (μM)	IC ₅₀ AChE (μM)	CNS perm ^a (PAMPA)	cLogP ^b	HSA ^a (% unbound)
1		324.15	>10	0.5	3.2	3.69	12
2		354.16	0.7	3.6	2	3.73	15
3		354.16	1	0.1	2.3	3.73	10
4		408.13	2.7	>5	0.7	4.84	33
5		330.19	3.4	0.3	2.8	3.66	17
6		352.18	3.6	0.2	3.1	4.68	4
7		384.17	2	0.3	1.8	3.75	9
8		325.14	0.5	7	1.9	2.86	28
9		352.18	>5	2.5	3	4.73	7
10		352.18	5	3.7	3.2	4.73	5
11		325.14	0.5	1.7	1.8	2.86	31
12		325.14	0.8	>5	1.9	2.86	28
13		343.13	0.6	>5	1.3	2.65	31
14		343.13	0.9	>5	2	3.1	21
15		392.13	5	>5	2.2	4.94	7
16		337.42	>5	>5	NA	NA	NA

a- Measured values, see details in SI; b-calculated value using StarDrop software

1
2
3 A summary of the dual nSMase2/AChE inhibition SAR from our optimization
4 efforts is summarized in Figure 2. Key points are as follows: (1) replacement of nitrogen
5 in the furoindoline ring of the validated hit yields **1** (phensvenine), which is a dual
6 inhibitor showing weak nSMase2 inhibition ($IC_{50} > 10 \mu\text{M}$) but potent AChE ($IC_{50}=0.5$
7 μM) inhibition; ⁴² (2) phenserine, a commercially available potent AChE inhibitor,
8 displays loss of nSMase2 inhibitory activity (IC_{50} (not depicted) $>50 \mu\text{M}$); (3) substitution
9 in the 3-position of carbamate ring favors enhanced AChE inhibition as seen in
10 compound **3** compared to compound **2**; (4) the 4-pyridyl ring in the carbamate group
11 leads to **8**, a dual inhibitor with ~14-fold selectivity for nSMase2 inhibition ($IC_{50} = 0.5$
12 μM) over AChE inhibition ($IC_{50} = 7 \mu\text{M}$); and (5) the 3-pyridyl carbamate compound **11**
13 was a dual inhibitor with ~3-fold selectivity for nSMase2 ($IC_{50}=0.5 \mu\text{M}$) and AChE
14 ($IC_{50}=1.7 \mu\text{M}$) inhibition. The mode of inhibition by the dual inhibitors (shown below) of
15 both enzymes allow for comparison dual activity using IC_{50} values.^{39,41} Based on the
16 SAR, the two dual inhibitors, **8** and **11**, with 10- and 3-fold selectivity for nSMase2
17 inhibition over AChE, respectively, were further evaluated in in vitro and in vivo assays
18 for exosomal tau release.
19
20
21
22
23
24
25
26
27
28
29
30



1
2
3 **Figure 2.** Key structure-activity relationship (SAR) control elements for inhibition of
4 nSMase2 (blue highlight) and AChE (yellow or green highlight) activity are indicated.
5
6
7

8 **Mechanism of AChE and nSMase2 inhibition by the novel furoindoline**
9 **compounds.** To determine the type of nSMase2 inhibition by compounds **8** and **11**,
10 kinetics assays were performed. As shown in **Figures 3a and 3b**, increasing
11 concentrations of compounds **8** and **11** resulted in decreasing K_m (the Michaelis
12 constant) values as well as concomitant decreases in V_{max} (the maximum rate)
13 indicative of a uncompetitive mechanism of inhibition of nSMase2.⁴³ Thus, it can be
14 concluded that both compounds bind to the enzyme distal from the active site and can
15 inhibit enzyme-substrate cleavage.
16
17
18
19
20
21

22 Molecular docking analysis (see the SI for details) was performed using a
23 recently published crystal structure of the nSMase2 catalytic domain (pdb: 5UVG).⁴⁴ We
24 found that both **8** and **11** could bind to nSMase2 at the distal DK-switch (Asp-Lys) site
25 away from the substrate sphingomyelin site, and thus in concordance with the kinetic
26 analysis, could be an uncompetitive inhibitor of the enzyme through modulation of the
27 DK-switch. This is similar to what we have previously published with the known
28 nSMase2 inhibitor cambinol, which was also shown by molecular docking and
29 simulation to bind the nSMase2 catalytic domain in the DK-switch region and prevent
30 enzyme activation by likely keeping the switch in the 'off' position.¹⁴ Molecular
31 Dynamics (MD) simulation was performed to determine the binding free energy of
32 compound **8** binding to nSMase2. Compound **8** stays at the DK-switch site of nSMase2
33 through the 50 ns simulation with an estimated binding energy of -14.3 kcal/mol. An
34 AMBER16 package was used to perform the MD simulation.
35
36
37
38
39
40
41
42
43
44

45 Kinetic studies of AChE inhibition by Phenserine was shown to be in a mixed
46 type manner (competitive/uncompetitive), we assumed that likewise the dual inhibitor
47 compounds **8** and **11** would bind to active site of AChE and show mixed inhibition.^{41, 42}
48
49
50
51
52
53
54
55
56
57
58
59
60

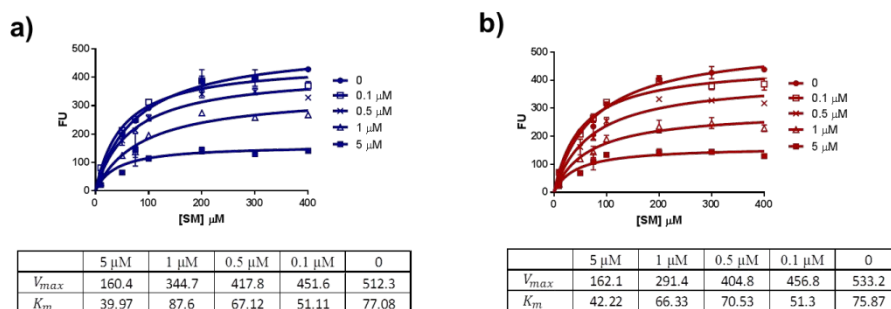
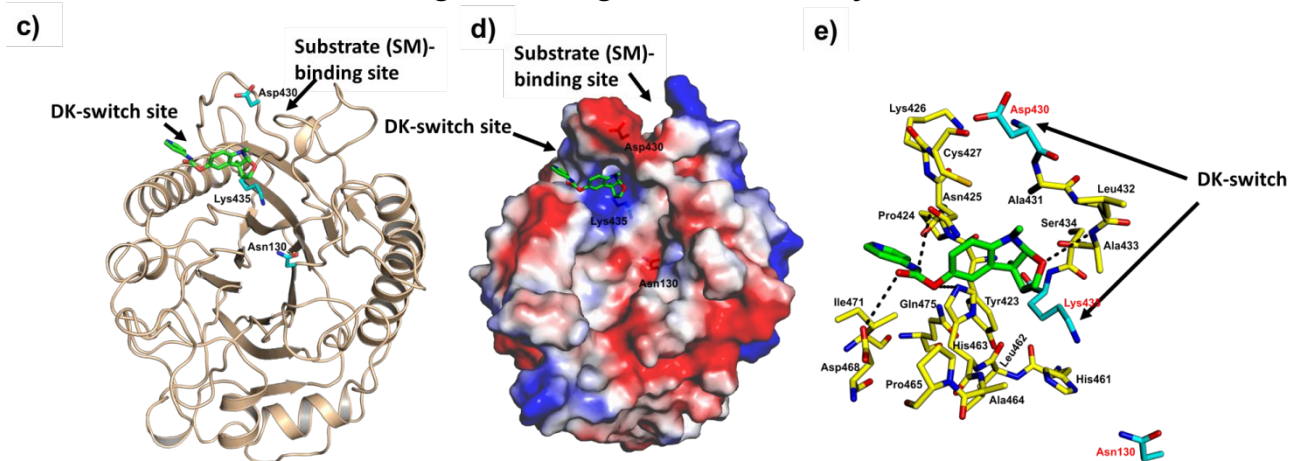
Kinetics of nSMase2 enzyme inhibition by **8** and **11***In silico* modeling of **8** binding with nSMase2 enzymatic domain

Figure 3. Mechanism of nSMase2 inhibition by compounds **8** and **11**. Kinetics of enzyme inhibition by compounds **8** (a) and **11** (b) are shown. The rate of the reaction is plotted against substrate concentration at four different concentrations of the inhibitors; corresponded values for V_{max} and K_m are presented in the tables below the graphs. c) Modeling of **8** and **11** (green) binding to catalytic domain of nSMase2 predicts compound binding preferably near DK-switch site than substrate binding site. d) Molecular surface representation of the nSMase2 catalytic domain with **8** and **11** (green) bound near the DK-switch; the color representations are blue for positive charge, red for negative charge and white for neutral charge. e) The nSMase2 residues (yellow) within 5 Å radius surrounding inhibitors **8** and **11** (green); H-bonding between the inhibitor and nSMase2 are shown in dashed lines (black).

In vitro inhibition of tau seed propagation by dual nSMase2/AChE inhibitors. We previously developed a cell culture system based on a well-known tau RD biosensor cell line (tau biosensors) for testing inhibitors of tau propagation.¹⁴ Using known nSMase2 inhibitors cambinol and GW4869, we had demonstrated the role of the nSMase2-dependent pathway of EV biogenesis in tau transmission from donor to recipient cells in

this non-neuronal cell model using two different in vitro assays – the Donor plus Recipient (D+R) assay and the EV-mediated transfer (EMT) assay.¹⁴

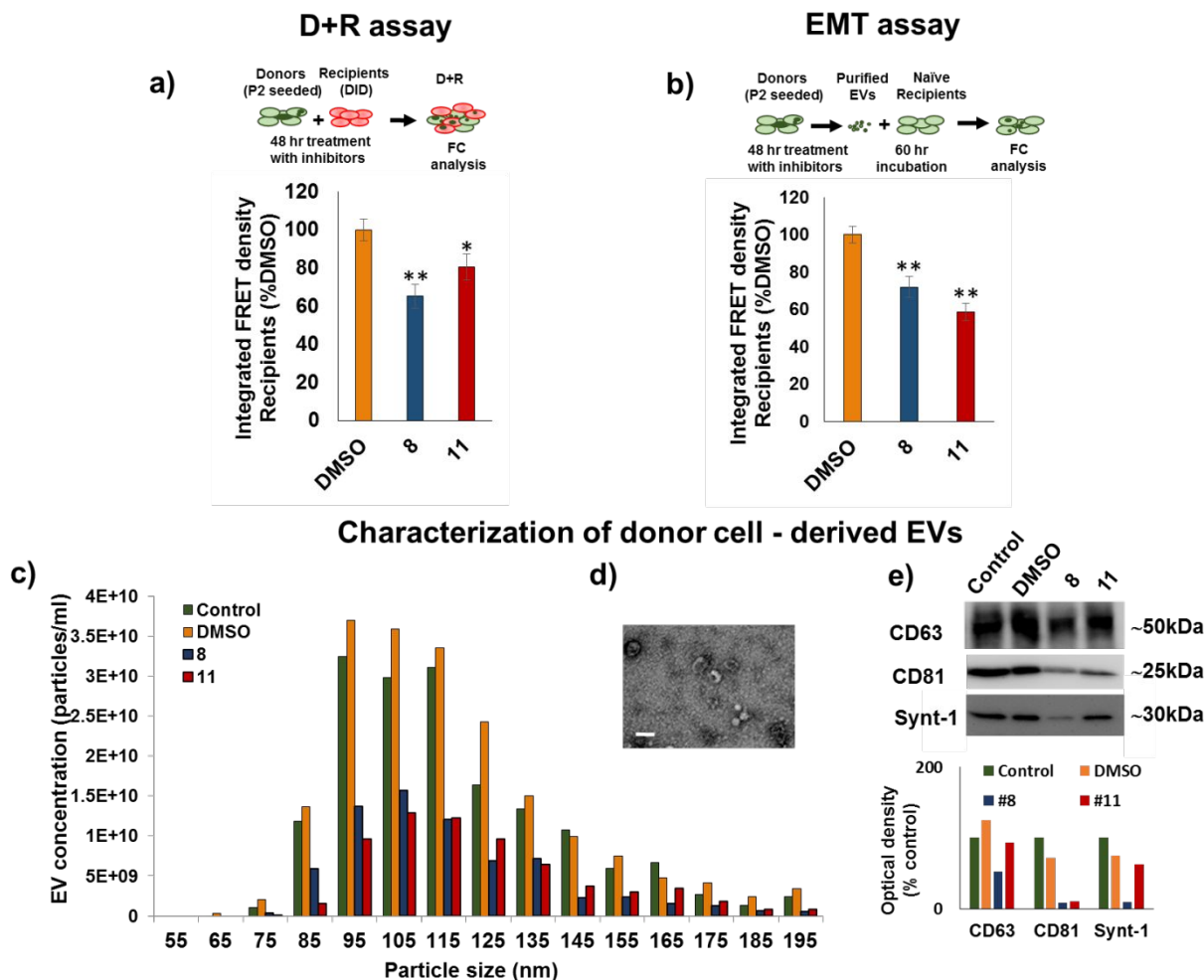


Figure 4. Dual nSMase2/AChE inhibitors **8** and **11** suppress tau propagation from donor to recipient cells in vitro. The assay scheme for each assay is presented at the top of the figure. a) Donor plus recipient (D+R) assay results are shown. Compounds **8** and **11** at a concentration of 20 μ M or a corresponding volume of DMSO were added to the D+R cultures for 48 hrs. Levels of FRET signal were analyzed in recipient cells using flow cytometry. Combined data from three independent experiments are presented. b) EV-mediated tau seed transfer (EMT) assay results are shown. Compounds **8** and **11** at 20 μ M concentration or DMSO were added to donor cell culture medium and then donor cell-derived EVs were purified and transfected to recipient cells. Levels of FRET signal were analyzed in recipient cells using flow cytometry. Four technical replicates were used for each experimental condition. Combined data from three independent experiments is presented. The histograms represent integrated FRET density per each treatment group (mean \pm SEM). c) Size distribution and concentrations of the donor-derived EV samples were analyzed by Tunable Resistive

1
2
3 Pulse Sensing (TRPS). d) Donor-derived EVs were imaged using transmission electron
4 microscopy (TEM). e) Western blot (WB) representative images for exosomal markers
5 are shown. The same volume of EV fractions derived from a similar number of donor
6 cells or control tau biosensor cells treated with Lipofectamine 2000 (Control) were
7 loaded per well and probed against exosomal markers CD63, CD81, and Syntenin-1.
8 Densitometry analysis is shown below the WB image. Statistics were performed using
9 One-way ANOVA with post hoc Bonferroni and Holm multiple comparison test was used
10 for statistical analysis: * $p < 0.05$, ** < 0.01 .
11
12
13

14 The principles of the D+R and EMT assays are presented in schematic form in
15 **Figures 4a** and **4b**, respectively. Our data demonstrates that treatment with **8** or **11** at
16 a concentration of 20 μM significantly suppresses tau seed transfer from donor to
17 recipient cells in the D+R and EMT assays (**Figures 4a, 4b** and **Supplementary**
18 **Figure 10**). Shuttling by tau-bearing EVs is not the only pathway of tau seed transfer
19 between cells in vivo or when donor and recipient cells are growing together in vitro, as
20 in the D+R assay. In contrast, the EMT assay lets us isolate the effect of the inhibitors
21 on EV-mediated tau seed transmission, which can explain the profound difference in the
22 magnitude of FRET fluorescence density by dual nSMase2/AChE inhibitor **11** between
23 the assays - 19.5% decrease from dimethyl sulfoxide (DMSO) treated cells in D+R
24 assay and 41.3% decrease in EMT assay.
25
26
27
28
29
30
31
32

33 We characterized EVs purified from the seeded donor cells growing in the
34 presence of our dual inhibitor compounds **8** and **11** or DMSO control. Successful
35 purification of EVs was confirmed by tunable resistive pulse sensing (TRPS) (**Figures**
36 **4c**), transmission electron microscopy (TEM) (**Figures 4d**), and western blotting
37 analysis with known exosomal markers (**Figures 4e**). Treatment with dual
38 nSMase2/AChE inhibitors **8** or **11** did not affect EV size distribution, but decreased the
39 concentrations of exosomal-type small EVs (**Figures 4c**). Levels of exosomal markers
40 CD63, CD81, and syntenin-1 were reduced in EVs purified from **8** and **11** treated cells
41 in comparison with the DMSO treated donors (**Figures 4e**). Relatively high suppression
42 of tau transfer by **11** compared to **8** in the EMT assay may be related to the greater
43 AChE inhibitory activity of **11** in conjunction with its nSMase2 inhibition and the role of
44 dual inhibitory activity in exosome-mediated transfer of tau seeds.³⁸ Interestingly, in
45 pilot testing using the (+) enantiomer of **8** and **11** in the EMT assay, we did not see any
46 suppression of EV-mediated tau seed transfer when compared to the (-) enantiomer.
47
48
49
50
51
52
53
54
55
56
57
58
59
60

1
2
3 Cell viability and/or rate of proliferation may have an effect on tau seed transfer
4 from donor to recipient cells through different mechanisms. Thus, we evaluated effects
5 of tau seeding and treatment with nSMase2/AChE inhibitors on donor cell number and
6 viability. Twenty-four hour exposure to AD human brain synaptosomal extracts
7 decreased the rate of the donor cell survival in the next passage compared to cells
8 treated with lipofectamine 2000 (**Supplementary Figure 11**). We have not determined
9 the specific mechanisms of cell death in tau-seeded donor cultures. It is possible that a
10 subset of tau-bearing EVs affected by nSMase2 inhibitors are apoptotic exosome-like
11 vesicles (AEVs) that - in contrast to apoptotic bodies - represent a subtype of exosomes
12 originating from multivesicular endosomes (MVE) at the early apoptotic phase. AEV
13 biogenesis is controlled by the ESCRT-independent sphingosine1-phosphate
14 (S1P)/S1PRs signaling pathway, and can be partially inhibited by nSMase2 inhibitor
15 GW4869.⁴⁵ Interestingly, AChE inhibitors are known to protect different cell types,
16 including HEK293T, from apoptosis,⁴⁶ and thus dual inhibitor **11** with greater AChE
17 inhibition could potentially indirectly suppress AEV production. However, treatment of
18 donor cells with **11** for 48 hours didn't affect donor cell numbers or survival compared to
19 DMSO or to compound **8** treated donor cells (**Supplementary Figures 11a and 11b**).
20 We also hypothesize that other factors may contribute to the greater effect of **11** on tau
21 seed transfer in the EMT assay. A recent report suggests that intracellular uptake of tau
22 can be mediated by the muscarinic acetylcholine receptors (mAChR) M1 and M3.³⁸
23 Thus, accumulation of tau oligomers in the synapse may exacerbate the cholinergic
24 deficit in AD through suppression of ACh uptake via mAChR M1/M3 receptors on
25 postsynaptic terminals. Based on similar reasoning, inhibition of AChE could have a
26 direct effect on tau seed uptake through the increased levels of ACh in the synapse and
27 postsynaptic M1/M3 receptor occupancy.

28
29
30
31
32
33
34
35
36
37
38
39
40
41
42
43
44
45
46 Our preliminary experiments at 20 μ M using rivastigmine, a potent AChE (but
47 with no nSMase2 activity) inhibitor, reveals that inhibition of AChE may partially
48 suppress EV-mediated transfer and uptake of tau seeds by recipient cells
49 (**Supplementary Figures 12**). We have previously published on cambinol, an nSMase2
50 inhibitor (IC₅₀ = 7.7 μ M but no AChE activity), that shows inhibition of tau seed transfer
51 in the EMT assay.¹⁴ The novel dual inhibitors **8** and **11** have both nSMase2/AChE
52
53
54
55
56
57
58
59
60

inhibitory activities in the same molecule and show suppression of tau transfer (**Figures 4b**). Thus, these dual nSMase2/AChE inhibitors **8** and **11** are agents that could be developed to efficiently target both enzymes in the brain and suppress tau propagation.

Brain pharmacokinetics for lead compounds. Our goal was to identify brain permeable dual nSMase2/AChE inhibitor analogs for further testing. We therefore performed pharmacokinetic (PK) analysis on the leads **8** and **11** to determine brain permeability using wild type mice. The compounds, whose brain permeability have not been previously described, were subcutaneously (SQ) injected at a relatively high dose of 20 mg per kg of body weight (mpk) to determine brain penetrance. Brain and plasma samples were collected 1, 2, and 4 hours after dosing. Our PK analysis revealed that **8** and **11** reached peak brain levels (C_{max}) around one hour after SQ dosing and brain levels were detectable for both compounds 4 hours after injection (**Figure 5a**).

Brain pharmacokinetics

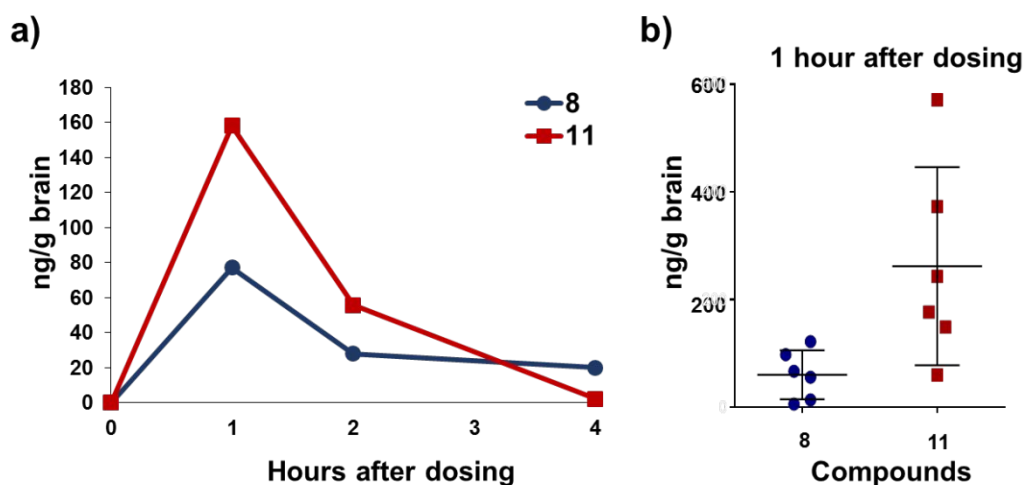


Figure 5. Pharmacokinetic analysis for lead compounds **8** and **11**. a) Mice were subcutaneously (SQ) injected with 20 mg/kg of compound **8** or **11**; animals were sacrificed 1, 2, and 4 hours after dosing ($n=1$ animal per time point). b) Mice were dosed as in (a), but $n = 6$ per compound and sacrificed 1 hour after dosing. Compound levels in brain tissue were analyzed using a LC-MS/MS method.

To carefully evaluate brain compound levels at the C_{max} (1 hour) time point, 20 mpk SQ dosing of compounds **8** and **11** was performed again using 6 mice per group. Average brain level of the compounds at the peak was equal to 61 ng/g ($\sim 0.2 \mu\text{M}$) and 262 ng/g ($\sim 0.8 \mu\text{M}$) for compounds **8** and **11**, respectively (**Figure 5b**). This data

1
2
3 confirmed good brain permeability of the lead compounds as was predicted by *in silico*
4 and PAMPA analysis described earlier (**Table 1**). Compound **11** showed higher average
5 brain levels compared to **8**, and the brain levels corresponded to ~ 2-fold IC₅₀ for
6 nSMase2 and ~0.5-fold for AChE.
7
8
9

10 **Inhibition of brain EV release by the dual nSMase2/AChE inhibitors in a rapid in**
11 **vivo assay.** The chronic inflammation that is reported in AD and tauopathy models is
12 characterized by elevated levels of pro-inflammatory cytokines in brain parenchyma,
13 including interleukin 1 β (IL1 β), known to induce nSMase2 activity through the IL1-
14 Receptor 1 (IL1-R1).⁴⁷ Neuroinflammation and upregulation of IL1 β signaling is linked
15 with an early stage of tauopathy development; blocking of IL1 β signaling in the 3xTg
16 mouse AD model attenuates tau pathology and rescues cognition.⁴⁸⁻⁵⁰ It was
17 demonstrated that striatal injection of IL1 β to wildtype mice induced release of
18 astrocyte-derived EVs into the blood, resulting in peripheral acute cytokine responses⁵¹
19 which can be suppressed by pre-treatment with nSMase2 inhibitors.³⁴⁻³⁵
20
21
22
23
24
25
26
27

28 In order to rapidly test our dual nSMase2 inhibitors in vivo, we used the Tau
29 P301S (PS19 line) tauopathy mouse model.⁴⁸ For our in vivo assay there were 4
30 groups: group I (control) received SQ injection of vehicle (DMSO) and
31 intracerebroventricular (ICV) injection of another vehicle (0.0006% BSA in PBS, pH 7.4)
32 an hour after SQ treatment; group II (IL1 β) received SQ injection of vehicle and
33 unilateral ICV injection of 0.2 ng of IL1 β an hour later; group III (**8**/IL1 β) – SQ treatment
34 with 20 mg/kg of **8** and ICV injection of 0.2 ng of IL1 β ; group IV - SQ treatment with 20
35 mg/kg of **11** and ICV injection of 0.2 ng of IL1 β . The one-hour interval between
36 treatment with the inhibitors and IL1 β ICV injection was chosen based on the brain PK
37 analysis presented above. All animals were sacrificed at 3 hours after compound or
38 vehicle treatment and 2 hours after ICV injection of IL1 β . Brain EVs were purified as
39 previously described.⁵²
40
41
42
43
44
45
46
47
48

49 Size distribution and concentration of brain EVs were analyzed using the TRPS
50 method. There were no significant differences in EV size distribution between
51 experimental groups (**Figure 6a**). As previously reported,⁵² the collected fraction (F2)
52 consists mostly of small exosome-size EVs with a mode equal to 80 \pm 5 nm based on
53 TRPS analysis. A high abundance of exosome-sized EVs was confirmed by TEM
54
55
56
57
58
59
60

analysis (**Figure 6c**). As expected we found that ICV injection of IL1 β significantly increased the concentration of small EVs (size 50-150 nm) purified from the brain, more than 2 times that of the control (**Figure 6b**). Dual nSMase2/AChE inhibitors **11** suppressed IL1 β -induced exosomal release to the control level (**Figure 6b**), while the less brain-permeable dual inhibitor **8** did not induce the same level of suppression.

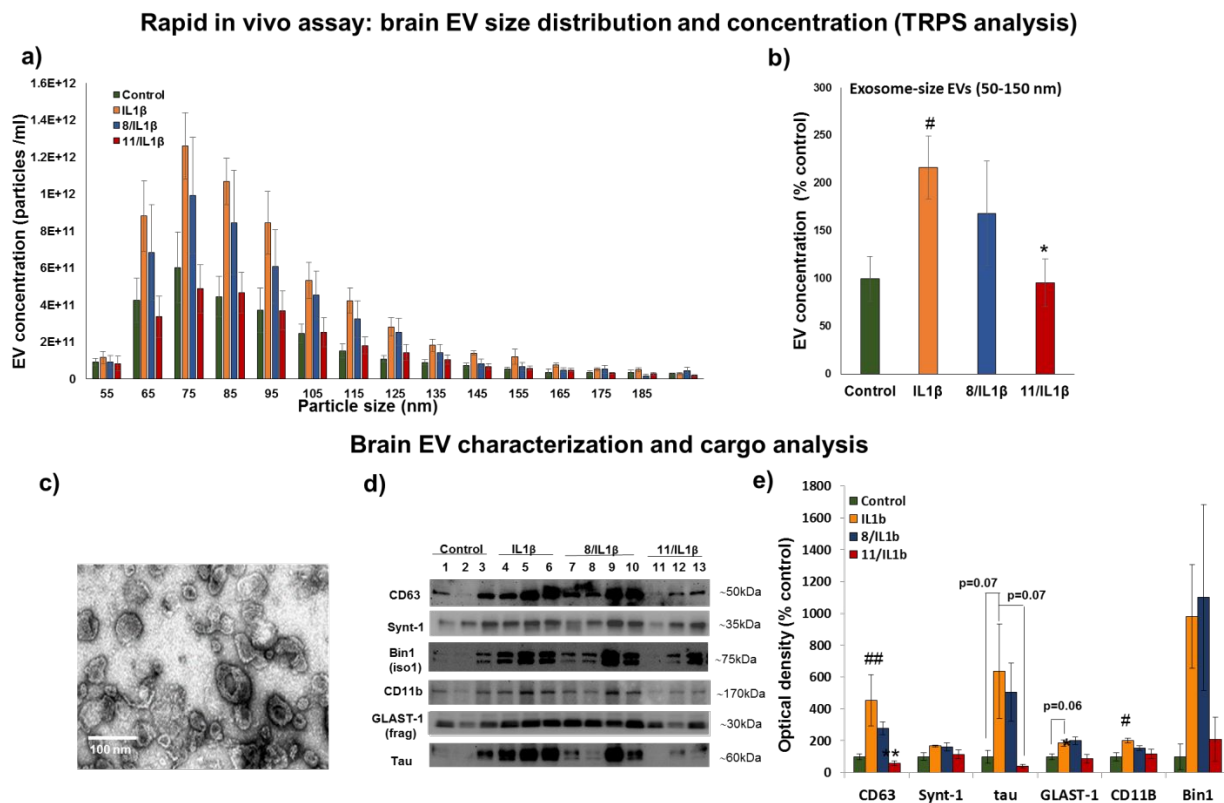


Figure 6. Dual nSMase2/AChE inhibitor **11** diminished IL1 β -induced brain EV release in the rapid in vivo assay. Tau P301S (line PS19) mice were treated with compound **8** or **11** subcutaneously (SQ) at 20 mg/kg one hour before IL1 β injection (unilateral ICV injection of 0.2 ng). Two hours after IL1 β injection, brain tissue was collected and used for brain EV isolation. a) Size distribution and concentrations of the brain EV samples were analyzed by Tunable Resistive Pulse Sensing (TRPS). b) Average concentrations of 50-150 nm size EVs from each treatment condition were compared. c) A representative transmission electron microscopy (TEM) image of the brain EV fraction is shown. d) Representative images of western blot (WB) analysis of EV fractions from individual animals is shown; membranes were probed against exosomal markers (CD63 and syntenin-1), tau protein, and cell-type specific markers (astrocytic glutamate-aspartate transporter GLAST1, microglia marker CD11b, and neuronal isoform of Bridging Integrator 1, BIN1). e) Densitometry analysis of the WB images is shown. Histograms represent average relative signal intensity per each treatment group (mean \pm SEM). Statistical analysis was performed using one-way ANOVA with post hoc

1
2
3 Bonferroni and Holm multiple comparison tests: #- $P < 0.05$ and ## - $P < 0.01$ compared
4 to control group, treated with vehicles for SQ and ICV injections, * - $P < 0.05$ and ** - P
5 < 0.01 compared to IL1 β group.
6

7 Biochemical analysis of brain-derived EVs (**Figures 6d & 6e**) confirmed that
8 pretreatment with lead compound **11** led to a significant reduction of exosomal marker
9 CD63 in exosome-enriched F2 fractions compared to the group treated only with IL1 β .
10 In contrast to significant changes in common exosomal marker CD63, levels of
11 syntenin-1, a marker of a specific exosomal subpopulation generated through the
12 Syndecan-Syntenin-ALIX pathway⁵³ were not different between the groups (**Figures 6d**
13 **& 6e**). These results confirm that IL1 β stimulation and nSMase2 inhibition have effects
14 on specific populations of exosomes.
15
16
17
18
19
20

21 Our data suggest that the nSMase2-dependent pathway of exosome biogenesis
22 is involved in tau-bearing exosome production in PS19 mice. Tau levels in the F2
23 fraction showed a strong trend of being elevated in animals treated with IL1 β , with the
24 average tau level being around 6 times higher in the IL1 β -treated group compared to
25 the control group (**Figures 6d & 6e**). Pretreatment with **11** significantly reduced IL1 β -
26 induced tau release by exosomes. The lead compound **8** was less effective in this
27 study. The known variability of tau load between PS19 mice likely accounts for the lack
28 of statistical significance despite the high magnitude of tau changes.
29
30
31
32
33
34

35 Multiple brain cell types express IL1-R1, including subpopulations of neurons,
36 astrocytes, choroid plexus cells and ependymal cells;⁵⁴ thus, the nSMase2-mediated
37 exosomal release by different types of brain cells can be affected differently in response
38 to acute increases in intracerebral IL1 β concentration. We used a couple of cell-type
39 specific markers to assess the origin of the IL1 β /nSMase2 sensitive exosomal
40 population. We found that levels of astrocytic glutamate-aspartate transporter (GLAST)
41 and microglial marker CD11b were significantly elevated in F2 fractions isolated from
42 IL1 β -treated animals. GLAST is known to be sensitive to papain, the enzyme we used
43 for gentle brain tissue dissociation. Therefore, we used a 30 kDa fragment of GLAST
44 instead of full-length protein for the analysis.⁵⁵ Pretreatment with the dual
45 nSMase2/AChE inhibitor **11** significantly reduced the level of astrocyte-derived
46 exosomes and showed the same trend for microglia-derived exosomes, but the
47
48
49
50
51
52
53
54
55
56
57
58
59
60

1
2
3 difference in CD11b levels between IL1 β and 11/IL1 β groups was not significant
4 (**Figures 6d & 6e**). This finding correlates with previously demonstrated IL1 β -induced
5 nSMase2-mediated production of astrocyte-derived exosomes in wild type mice.³⁴⁻³⁵
6
7 Microglia play an important role in tau spread,^{15, 55} and inhibition of microglial nSMase2-
8 dependent
9
10
11
12
13
14
15
16
17
18
19
20
21
22
23
24
25
26
27
28
29
30
31
32
33
34
35
36
37
38
39
40
41
42
43
44
45
46
47
48
49
50
51
52
53
54
55
56
57
58
59
60

Microglia play an important role in tau spread,^{15, 55} and inhibition of microglial nSMase2-dependent
exosome release suppresses tau propagation in mouse models.¹⁵ The low levels of microglia response in our rapid in vivo assay may be attributed to saturation of microglia responses in 5-6 month old PS19 mice. Microglia activation is already detectable in 3 month old PS19 mice and precedes astrogliosis.⁴⁸

Recently, Bridging Integrator 1 (BIN1), a known genetic risk factor for AD, was connected to tau seed release through exosomes in human AD and male PS19 mice.⁵⁶ We analyzed levels of BIN1 in our F2 samples. Neuronal BIN1 isoform 1, but not microglia specific isoform 2, were highly enriched in the F2 fractions (**Figure 6d**). As in the case of exosomal tau, we found a high magnitude increase in exosome-associated BIN1 upon IL1 β stimulation that was lower in the compound **11** treated group, but no statistically significant changes were found due to the high variability of individual levels of BIN1 within each group (**Figure 6d**). This data suggests that nSMase2 and BIN1 could be a part of the same exosomal pathway responsible for tau release and spread in AD.

Overall, our rapid in vivo assay results demonstrate the effectiveness of novel dual AChE/nSMase2 inhibitor **11** in suppression of IL1 β -induced release of tau-bearing exosomes in a tauopathy model.

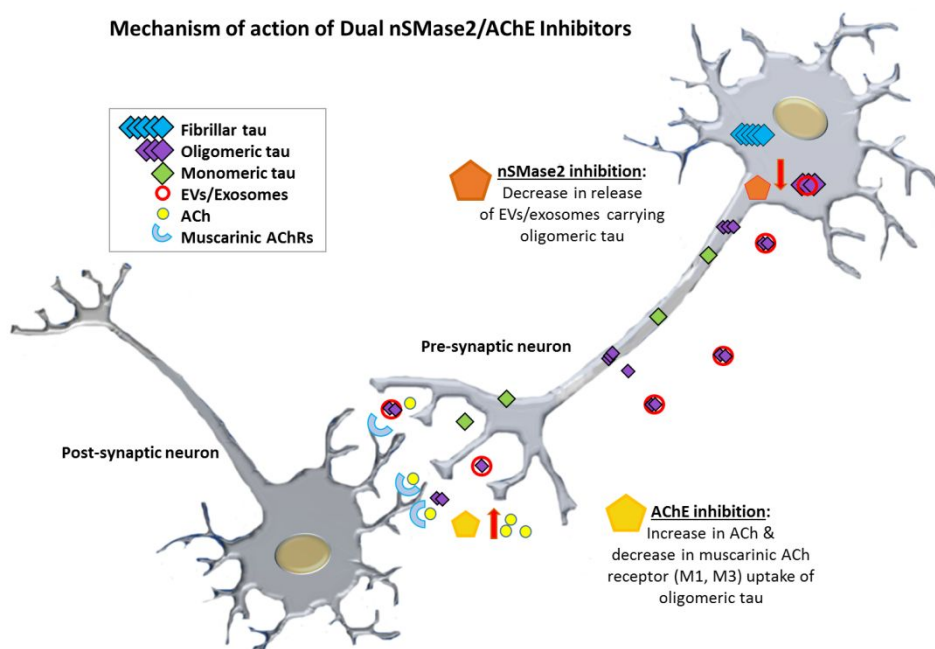


Figure 7. A putative mechanism for dual nSMase2/AChE inhibition and suppression of EV/exosome-mediated propagation of tau pathology wherein nSMase2 inhibition suppresses exosome biogenesis while AChE inhibition reduces exosome uptake and cholinergic support.

Our discovery of a novel class of potent nSMase2/AChE dual inhibitors presents an opportunity for further evaluation and development of these agents as a new therapeutic approach for the treatment of Alzheimer's disease. Our data supports the ability of the dual inhibitors to suppress tau propagation in vitro and release of tau carrying exosomes in vivo in an AD model. These dual nSMase2/AChE inhibitors would enhance cholinergic synaptic plasticity, reduce neuroinflammation,³⁷ and most importantly suppress exosome-mediated tau propagation and tau uptake mediated through the M1/M3 muscarinic ACh receptors.^{38, 57-59} This combination effect is unique, has not been evaluated previously in the disease and clearly differentiate these agents from currently available AChE inhibitors for the treatment of AD. In concert, these mechanisms of action have the potential to not only address symptoms of AD by enhancing cholinergic activity but also to suppress cell-to-cell tau propagation, (**Figure 7**), significantly altering an underlying cause of AD and thus be truly disease-modifying.

METHODS

Compound Synthesis. Unless stated otherwise, reactions were conducted in flame-dried glassware under an atmosphere of N₂ and commercially obtained reagents were used as received. Sodium hydride, boron tribromide, boron trichloride, phenyl isocyanate, *N,N'*-disuccinimidyl carbonate (**29**), cyclohexyl isocyanate, 3,5-dimethylphenyl isocyanate, 3,5-dimethoxyphenyl isocyanate, 3-aminopyridine (**33**), 4-aminopyridine (**32**), and 4-(trifluoromethyl)aniline (**37**) were obtained from Sigma-Aldrich. Hydrazine (**17**), 4-methoxyphenyl isocyanate, 3-methoxyphenyl isocyanate, and *N*-ethylmethylamine (**37**) were obtained from Oakwood Products, Inc. 4-(trifluoromethyl)phenyl isocyanate and 3-amino-5-fluoropyridine (**35**) were obtained from Combi-Blocks. Methyl iodide was obtained from Alfa Aesar. Reaction temperatures were controlled using an IKA Mag temperature modulator, and unless stated otherwise, reactions were performed at room temperature (approximately 23 °C). Thin-layer chromatography (TLC) was conducted with EMD gel 60 F254 pre-coated plates (0.25 mm for analytical chromatography and 0.50 mm for preparative chromatography) and visualized using a combination of UV, anisaldehyde, iodine, and potassium permanganate staining techniques. Silicycle Siliaflash P60 (particle size 0.040–0.063 mm) was used for flash column chromatography. ¹H NMR spectra were recorded on Bruker spectrometers (500 MHz) and are reported relative to residual solvent signals. Data for ¹H NMR spectra are reported as follows: chemical shift (δ ppm), multiplicity, coupling constant (Hz), integration. Data for ¹³C NMR are reported in terms of chemical shift (125 MHz). ¹⁹F NMR spectra were recorded on Bruker spectrometers (at 376 MHz) and reported in terms of chemical shifts (δ ppm). Data for IR spectra were recorded on a Perkin-Elmer UATR Two FT-IR spectrometer and are reported in terms of frequency absorption (cm⁻¹). DART-MS spectra were collected on a Thermo Exactive Plus MSD (Thermo Scientific) equipped with an ID-CUBE ion source and a Vapor Interface (IonSense Inc.). Both the source and MSD were controlled by Excalibur software v. 3.0. The analyte was spotted onto OpenSpot sampling cards (IonSense Inc.) using volatile solvents (e.g. chloroform, dichloromethane). Ionization was accomplished using UHP He (Airgas Inc.) plasma with no additional ionization agents. The mass calibration was carried out using Pierce LTQ Velos ESI (+) and (-) Ion calibration

1
2
3 solutions (Thermo Fisher Scientific). Optical rotations were measured with a Rudolph
4 Autopol III Automatic Polarimeter. Any modification of the conditions shown in the
5 representative procedures are specified in the corresponding schemes. The detailed
6 methods for synthesis of the compounds are included in the Supporting Information.
7
8
9

10
11 **Enzyme activity and kinetic analysis assay.** To evaluate nSMase2 inhibitory activity
12 of tested compounds, cell lysates from HEK293T cells over-expressing human
13 nSMase2 were used as the source of the nSMase2 enzyme.³⁴ The enzyme activity was
14 measured with or without inhibitor treatment using the Amplex Red Sphingomyelinase
15 activity assay.⁴² For acetylcholinesterase (AChE) assay we used human AChE
16 (Sigma). The enzyme activity was measured with or without inhibitor treatment using the
17 Amplex Red assay kit (Thermo Fisher A12217). The reaction was monitored for 60 min
18 and read at 530/590 nm. The detail methods for enzyme activity analysis are included
19 in the Supporting Information.
20
21
22
23
24
25
26
27
28

29 **Modeling of compounds binding to SMase2.** Molecular docking analysis of
30 compounds was performed using the Swiss Dock server on our Area51 Work Area 51
31 R4 linux workstation. Molecular Dynamics (MD) simulation was performed to determine
32 the binding free energy of compound 8 binding to nSMase2. An AMBER16 package
33 was used to perform the MD simulation. The Antechamber module in AMBER was used
34 to generate the parameters for compounds. The SwissDock web server was used
35 to predict compound binding to nSMase2. The detail methods for modeling analysis
36 included in the Supporting Information.
37
38
39
40
41
42
43

44 **Parallel Artificial Membrane Permeability Assay (PAMPA).** To predict the potential
45 for brain permeability, a Regis Technologies analytical column connected to an Agilent
46 HPLC system was used. We used the IAM.PC.DD column for determination of the
47 retention time of a compound to calculate the predicted CNS permeability. The detail
48 methods for modeling analysis included in the Supporting Information.
49
50
51
52
53
54
55
56
57
58
59
60

1
2
3 **Human Serum Albumin (HSA) Binding Assay.** For HSA compound binding we use a
4 CHIRAL column immobilized with HSA on a Agilent HPLC system. The detail methods
5 for modeling analysis included in the Supporting Information.
6
7
8
9

10 **Preparation of brain-derived synaptosomal extracts.** Cryopreserved brain tissue
11 was obtained from University of California Irvine was used for preparation of the
12 synaptosomal fractions (P2 fractions, 'P2'). The detail methods for modeling analysis
13 included in the Supporting Information.
14
15
16
17

18 **Tau propagation assays.** We use the HEK293T Tau RD P301S FRET biosensor (tau
19 biosensor) for evaluation of the inhibitors in functional tau propagation "D+R" (Donors
20 plus Recipients) and EMT (EV-mediated transfer) assays. We have previously
21 published the detailed protocols and validation of the assays using known nSMase2
22 inhibitors GW4869 and cambinol.¹⁴ The detail methods for modeling analysis included
23 in the Supporting Information.
24
25
26
27
28
29

30 **Rapid *in vivo* assay and brain EV purification.** Using 5-6 month old male PS19 mice
31 expressing human tau with the P301S mutation under control of the murine prion
32 promoter intracerebroventricular (ICV) injections of IL-1 β with or without pre-treatment
33 with dual nSMase2/AChE inhibitor followed isolation of EVs. The *in vivo* experiments
34 were performed under an approved IACUC protocol. The detail methods for modeling
35 analysis included in the Supporting Information.
36
37
38
39
40
41

42 **Transmission electron microscopy (TEM).** For quality control purposes, small
43 amounts of purified brain- or tissue culture- derived EVs were fixed on a copper mesh in
44 glutaraldehyde/paraformaldehyde solution, stained with 2% uranyl acetate solution and
45 imaged on a JEOL 100CX electron microscope at 29,000X magnification.
46
47
48
49

50 **Tunable Resistive Pulse Sensing analysis.** Size distribution and concentrations of EV
51 samples were analyzed by Tunable Resistive Pulse Sensing (TRPS) method using the
52 qNano Gold instrument (Izon Science). NP100 nanopore (particle size range: 50-330
53
54
55
56
57
58
59
60

1
2
3 nm) and CPC100 calibration particles were used for the analysis. Data analysis was
4 performed using qNano instrument software.
5
6

7 **Immunoblot analysis of EV samples.** Electrophoresis of proteins was performed
8 using 10–20% Tris-Glycine gels in non-reducing (only for tetraspanins) or reducing (with
9 addition of DTT) conditions; proteins were then transferred to PVDF membrane and
10 probed with primary antibodies (Supporting Table 2) followed by HRP conjugated
11 secondary antibodies. Chemiluminescent signals were generated with Super Signal
12 West Femto substrate (Thermo Scientific Pierce 34095) and detected using a
13 BioSpectrum 600 imaging system and quantified using VisionWorks Version 6.6A
14 software (UVP; Upland, CA). The detail methods for modeling analysis included in the
15 Supporting Information.
16
17
18
19
20
21
22
23

24 **Statistical analysis.** All data was expressed as the mean \pm SEM. Significant
25 differences were determined by one-way ANOVA followed by Bonferroni and Holm
26 multiple comparison method using online web statistical calculator
27 (http://astatsa.com/OneWay_Anova_with_TukeyHSD). Only a subset of pairs relative to
28 the DMSO group were simultaneously compared. Values of * or #<0.05 and ** or
29 ##<0.01 were considered statistically significant.
30
31
32
33
34
35
36
37

38 **ASSOCIATED CONTENT**

39 The Supporting Information is available free of charge on the ACS Publications website.
40

41 Detailed experimental procedures, compound characterization data submitted as a
42 (PDF).
43
44
45
46
47
48
49
50
51
52
53
54
55
56
57
58
59
60

AUTHOR INFORMATION**Corresponding Authors***

Neil Garg, Ph.D.

Professor & Chair

UCLA Chemistry & Biochemistry

Email: neilgarg@chem.ucla.edu

 [0000-0002-7793-2629](https://orcid.org/0000-0002-7793-2629) ✓

Varghese John, Ph.D.

Professor of Neurology

PI, Drug Discovery Lab

UCLA Neurology

Email: vjohn@mednet.ucla.edu

 [0000-0001-7675-2426](https://orcid.org/0000-0001-7675-2426) ✓

Authors

Tina Bilousova, Ph.D. - University of California Los Angeles,

Department of Neurology

Drug Discovery Lab

3138 Reed Building

Los Angeles, CA, USA 90095

Bryan J. Simmons Ph.D. - University of California Los Angeles,

Dept. of Chemistry and Biochemistry

607 Charles Young Drive East

Los Angeles, CA, USA 90095

Rachel R. Knapp - University of California Los Angeles,

Dept. of Chemistry and Biochemistry

607 Charles Young Drive East

Los Angeles, CA, USA 90095

Chris J. Elias - University of California Los Angeles,

Department of Neurology

Drug Discovery Lab

3138 Reed Building

Los Angeles, CA, USA 90095

Jesus Campagna - University of California Los Angeles,

Department of Neurology

Drug Discovery Lab

3138 Reed Building

Los Angeles, CA, USA 90095

Sujyoti Chandra, Ph.D. - University of California Los Angeles,

1
2
3 Department of Neurology
4 Drug Discovery Lab
5 3138 Reed Building
6 Los Angeles, CA, USA 90095

7 **Samantha Focht** - University of California Los Angeles,
8 Department of Neurology
9 Drug Discovery Lab
10 3138 Reed Building
11 Los Angeles, CA, USA 90095

12 **Chunni Zhu, Ph.D.** - University of California Los Angeles,
13 Department of Neurology
14 Drug Discovery Lab
15 3138 Reed Building
16 Los Angeles, CA, USA 90095

17 **Kanagasabai Vadivel, Ph.D.** - University of California Los Angeles,
18 Orthopaedic Surgery
19 615 Charles Young Drive East
20 Los Angeles, CA, USA 90095

21 **Barbara Jagodzinska, Ph.D.** - University of California Los Angeles,
22 Department of Neurology
23 Drug Discovery Lab
24 3138 Reed Building
25 Los Angeles, CA, USA 90095

26 **Whitaker Cohn** - University of California Los Angeles,
27 Department of Neurology
28 Drug Discovery Lab
29 3138 Reed Building
30 Los Angeles, CA, USA 90095

31 **Karen H. Gyls, Ph.D.**- University of California Los Angeles,
32 School of Nursing
33 Gylys Lab
34 Los Angeles, CA, USA 90095

35 36 37 38 39 40 41 42 43 **Funding**

44
45 The work was supported by Mary S. Easton Center for Alzheimer's Disease Research
46 at UCLA to V.J.; National Institutes of Health (AG051386 to V.J.), and the National
47 Science Foundation (DGE-1144087 for B.J.S. and CHE-1464898 for N.K.G.) These
48 studies were supported by shared instrumentation grants from the NSF (CHE-1048804)
49 and the National Center for Research Resources (S10RR025631)
50
51
52
53
54
55
56
57
58
59
60

Notes

The authors declare no competing financial interests.

ACKNOWLEDGEMENTS

. The authors thank the funding sources that supported this work. We would like to thank W. W. Poon from UC Irvine for human autopsy brain samples, C. Rojas from John Hopkins School of Medicine for nSMase2-overexpressing HEK293 cells, and the UCLA Janis V. Giorgi flow cytometry and Brain Research Institute Electron microscopy core facilities.

REFERENCES

1. El-Hayek, Y. H.; Wiley, R. E.; Khoury, C. P.; Daya, R. P.; Ballard, C.; Evans, A. R.; Karran, M.; Molinuevo, J. L.; Norton, M.; Atri, A., Tip of the Iceberg: Assessing the Global Socioeconomic Costs of Alzheimer's Disease and Related Dementias and Strategic Implications for Stakeholders. *J Alzheimer's Dis* **2019**, *70* (2), 323-341.
2. Serrano-Pozo, A.; Frosch, M. P.; Masliah, E.; Hyman, B. T., Neuropathological alterations in Alzheimer disease. *Cold Spring Harb Perspect Med* **2011**, *1* (1), a006189.
3. Masters, C. L.; Bateman, R.; Blennow, K.; Rowe, C. C.; Sperling, R. A.; Cummings, J. L., Alzheimer's disease. *Nat Rev Dis Primers* **2015**, *1*, 15056.
4. Olivieri, P.; Lagarde, J.; Lehericy, S.; Valabrègue, R.; Michel, A.; Macé, P.; Caillé, F.; Gervais, P.; Bottlaender, M.; Sarazin, M., Early alteration of the locus coeruleus in phenotypic variants of Alzheimer's disease. *Ann Clin Transl Neurol* **2019**, *6* (7), 1345-1351.
5. Costandi, M., Ways to stop the spread of Alzheimer's disease. *Nature* **2018**, *559* (7715), S16-S17.
6. Selkoe, D. J.; Hardy, J., The amyloid hypothesis of Alzheimer's disease at 25 years. *EMBO Mol Med* **2016**, *8* (6), 595-608.
7. Hardy, J.; Selkoe, D. J., The amyloid hypothesis of Alzheimer's disease: progress and problems on the road to therapeutics. *Science* **2002**, *297* (5580), 353-6.
8. Nelson, P. T.; Alafuzoff, I.; Bigio, E. H.; Bouras, C.; Braak, H.; Cairns, N. J.; Castellani, R. J.; Crain, B. J.; Davies, P.; Del Tredici, K.; Duyckaerts, C.; Frosch, M. P.; Haroutunian, V.; Hof, P. R.; Hulette, C. M.; Hyman, B. T.; Iwatsubo, T.; Jellinger, K. A.; Jicha, G. A.; Kovari, E.; Kukull, W. A.; Leverenz, J. B.; Love, S.; Mackenzie, I. R.; Mann, D. M.; Masliah, E.; McKee, A. C.; Montine, T. J.; Morris, J. C.; Schneider, J. A.; Sonnen, J. A.; Thal, D. R.; Trojanowski, J. Q.; Troncoso, J. C.; Wisniewski, T.; Woltjer, R. L.; Beach, T. G., Correlation of Alzheimer disease neuropathologic changes with cognitive status: a review of the literature. *J Neuropathol Exp Neurol* **2012**, *71* (5), 362-81.
9. Johnson, K. A.; Schultz, A.; Betensky, R. A.; Becker, J. A.; Sepulcre, J.; Rentz, D.; Mormino, E.; Chhatwal, J.; Amariglio, R.; Papp, K.; Marshall, G.; Albers, M.; Mauro, S.; Pepin, L.; Alverio, J.; Judge, K.; Philiossaint, M.; Shoup, T.; Yokell, D.; Dickerson, B.; Gomez-Isla, T.; Hyman, B.; Vasdev, N.; Sperling, R., Tau positron emission tomographic imaging in aging and early Alzheimer disease. *Ann Neurol* **2016**, *79* (1), 110-9.
10. Pontecorvo, M. J.; Devous, M. D., Sr.; Navitsky, M.; Lu, M.; Salloway, S.; Schaerf, F. W.; Jennings, D.; Arora, A. K.; McGeehan, A.; Lim, N. C.; Xiong, H.; Joshi, A. D.; Siderowf, A.; Mintun, M. A.; investigators, F. A.-A., Relationships between flortaucipir PET tau binding and amyloid burden, clinical diagnosis, age and cognition. *Brain* **2017**, *140* (3), 748-763.
11. Kametani, F.; Hasegawa, M., Reconsideration of Amyloid Hypothesis and Tau Hypothesis in Alzheimer's Disease. *Front Neurosci* **2018**, *12*, 25.
12. Ishiki, A.; Okamura, N.; Furukawa, K.; Furumoto, S.; Harada, R.; Tomita, N.; Hiraoka, K.; Watanuki, S.; Ishikawa, Y.; Tago, T.; Funaki, Y.; Iwata, R.; Tashiro, M.; Yanai, K.; Kudo, Y.; Arai, H., Longitudinal Assessment of Tau Pathology in Patients with Alzheimer's Disease Using [18F]THK-5117 Positron Emission Tomography. *PLoS One* **2015**, *10* (10), e0140311.
13. Chiotis, K.; Saint-Aubert, L.; Rodriguez-Vieitez, E.; Leuzy, A.; Almkvist, O.; Savitcheva, I.; Jonasson, M.; Lubberink, M.; Wall, A.; Antoni, G.; Nordberg, A., Longitudinal changes of tau PET imaging in relation to hypometabolism in prodromal and Alzheimer's disease dementia. *Mol Psychiatry* **2018**, *23*(7), 1666-1673.
14. Bilousova, T.; Elias, C.; Miyoshi, E.; Alam, M. P.; Zhu, C.; Campagna, J.; Vadivel, K.; Jagodzinska, B.; Gylys, K. H.; John, V., Suppression of tau propagation using an inhibitor that targets the DK-switch of nSMase2. *Biochem Biophys Res Commun* **2018**, *499* (4), 751-757.

15. Asai, H.; Ikezu, S.; Tsunoda, S.; Medalla, M.; Luebke, J.; Haydar, T.; Wolozin, B.; Butovsky, O.; Kugler, S.; Ikezu, T., Depletion of microglia and inhibition of exosome synthesis halt tau propagation. *Nat Neurosci* **2015**, *18* (11), 1584-93.
16. Dinkins, M. B.; Dasgupta, S.; Wang, G.; Zhu, G.; Bieberich, E., Exosome reduction in vivo is associated with lower amyloid plaque load in the 5XFAD mouse model of Alzheimer's disease. *Neurobiol Aging* **2014**, *35* (8), 1792-800.
17. Dinkins, M. B.; Enasko, J.; Hernandez, C.; Wang, G.; Kong, J.; Helwa, I.; Liu, Y.; Terry, A. V., Jr.; Bieberich, E., Neutral Sphingomyelinase-2 Deficiency Ameliorates Alzheimer's Disease Pathology and Improves Cognition in the 5XFAD Mouse. *J Neurosci* **2016**, *36* (33), 8653-67.
18. Wheeler, D.; Knapp, E.; Bandaru, V. V.; Wang, Y.; Knorr, D.; Poirier, C.; Mattson, M. P.; Geiger, J. D.; Haughey, N. J., Tumor necrosis factor-alpha-induced neutral sphingomyelinase-2 modulates synaptic plasticity by controlling the membrane insertion of NMDA receptors. *J Neurochem* **2009**, *109* (5), 1237-49.
19. Tabatadze, N.; Savonenko, A.; Song, H.; Bandaru, V. V.; Chu, M.; Haughey, N. J., Inhibition of neutral sphingomyelinase-2 perturbs brain sphingolipid balance and spatial memory in mice. *J Neurosci Res* **2010**, *88* (13), 2940-51.
20. Tan, L. H.; Tan, A. J.; Ng, Y. Y.; Chua, J. J.; Chew, W. S.; Muralidharan, S.; Torta, F.; Dutta, B.; Sze, S. K.; Herr, D. R.; Ong, W. Y., Enriched Expression of Neutral Sphingomyelinase 2 in the Striatum is Essential for Regulation of Lipid Raft Content and Motor Coordination. *Mol Neurobiol* **2018**, *55* (7), 5741-56.
21. Stoffel, W.; Jenke, B.; Schmidt-Soltan, I.; Binczek, E.; Brodesser, S.; Hammels, I., SMPD3 deficiency perturbs neuronal proteostasis and causes progressive cognitive impairment. *Cell Death Dis* **2018**, *9* (5), 507.
22. Babenko, N. A.; Shakhova, E. G., Long-term food restriction prevents aging-associated sphingolipid turnover dysregulation in the brain. *Arch Gerontol Geriatr* **2014**, *58* (3), 420-6.
23. Filippov, V.; Song, M. A.; Zhang, K.; Vinters, H. V.; Tung, S.; Kirsch, W. M.; Yang, J.; Duerksen-Hughes, P. J., Increased ceramide in brains with Alzheimer's and other neurodegenerative diseases. *J Alzheimer's Dis* **2012**, *29* (3), 537-47.
24. Bandaru, V. V.; Troncoso, J.; Wheeler, D.; Pletnikova, O.; Wang, J.; Conant, K.; Haughey, N. J., ApoE4 disrupts sterol and sphingolipid metabolism in Alzheimer's but not normal brain. *Neurobiol Aging* **2009**, *30* (4), 591-9.
25. Trajkovic, K.; Hsu, C.; Chiantia, S.; Rajendran, L.; Wenzel, D.; Wieland, F.; Schwille, P.; Brugger, B.; Simons, M., Ceramide triggers budding of exosome vesicles into multivesicular endosomes. *Science* **2008**, *319* (5867), 1244-7.
26. Thery, C., Exosomes: secreted vesicles and intercellular communications. *F1000 Biol Rep* **2011**, *3*, 15.
27. Guo, B. B.; Bellingham, S. A.; Hill, A. F., The neutral sphingomyelinase pathway regulates packaging of the prion protein into exosomes. *J Biol Chem* **2015**, *290* (6), 3455-67.
28. Simon, D.; Garcia-Garcia, E.; Royo, F.; Falcon-Perez, J. M.; Avila, J., Proteostasis of tau. Tau overexpression results in its secretion via membrane vesicles. *FEBS Lett* **2012**, *586* (1), 47-54.
29. Polanco, J. C.; Scicluna, B. J.; Hill, A. F.; Gotz, J., Extracellular vesicles isolated from brains of rTg4510 mice seed tau aggregation in a threshold-dependent manner. *J Biol Chem* **2016**, *291*(24), 12445-66.
30. Wang, Y.; Balaji, V.; Kaniyappan, S.; Kruger, L.; Irsen, S.; Tepper, K.; Chandupatla, R.; Maetzler, W.; Schneider, A.; Mandelkow, E.; Mandelkow, E. M., The release and trans-synaptic transmission of Tau via exosomes. *Mol Neurodegener* **2017**, *12* (1), 5.
31. Fiandaca, M. S.; Kapogiannis, D.; Mapstone, M.; Boxer, A.; Eitan, E.; Schwartz, J. B.; Abner, E. L.; Petersen, R. C.; Federoff, H. J.; Miller, B. L.; Goetzl, E. J., Identification of preclinical Alzheimer's disease

1
2
3 by a profile of pathogenic proteins in neurally derived blood exosomes: A case-control study. *Alzheimer's*
4 *Dement* **2015**, *11* (6), 600-7.e1.

5 32. Abner, E. L.; Jicha, G. A.; Shaw, L. M.; Trojanowski, J. Q.; Goetzl, E. J., Plasma neuronal exosomal
6 levels of Alzheimer's disease biomarkers in normal aging. *Ann Clin Trans Neurol* **2016**, *3* (5), 399-403.

7 33. Saman, S.; Kim, W.; Raya, M.; Visnick, Y.; Miro, S.; Saman, S.; Jackson, B.; McKee, A. C.; Alvarez,
8 V. E.; Lee, N. C.; Hall, G. F., Exosome-associated tau is secreted in tauopathy models and is selectively
9 phosphorylated in cerebrospinal fluid in early Alzheimer disease. *J Biol Chem* **2012**, *287* (6), 3842-9.

10 34. Rojas, C.; Barnaeva, E.; Thomas, A. G.; Hu, X.; Southall, N.; Marugan, J.; Chaudhuri, A. D.; Yoo, S.
11 W.; Hin, N.; Stepanek, O.; Wu, Y.; Zimmermann, S. C.; Gadiano, A. G.; Tsukamoto, T.; Rais, R.; Haughey,
12 N.; Ferrer, M.; Slusher, B. S., DPTIP, a newly identified potent brain penetrant neutral sphingomyelinase
13 2 inhibitor, regulates astrocyte-peripheral immune communication following brain inflammation. *Sci Rep*
14 **2018**, *8* (1), 17715.

15 35. Rojas, C.; Sala, M.; Thomas, A. G.; Datta Chaudhuri, A.; Yoo, S. W.; Li, Z.; Dash, R. P.; Rais, R.;
16 Haughey, N. J.; Nencka, R.; Slusher, B., A novel and potent brain penetrant inhibitor of extracellular
17 vesicle release. *Br J Pharmacol* **2019**, *176* (19), 3857-3870.

18 36. Mehta, M.; Adem, A.; Sabbagh, M., New acetylcholinesterase inhibitors for Alzheimer's disease.
19 *Int J of Alzheimer's Dis* **2012**, *2012*, 728983.

20 37. Maurer, S. V.; Williams, C. L., The Cholinergic System Modulates Memory and Hippocampal
21 Plasticity via Its Interactions with Non-Neuronal Cells. *Front Immunol* **2017**, *8*, 1489.

22 38. Morozova, V.; Cohen, L. S.; Makki, A. E.; Shur, A.; Pilar, G.; El Idrissi, A.; Alonso, A. D., Normal and
23 Pathological Tau Uptake Mediated by M1/M3 Muscarinic Receptors Promotes Opposite Neuronal
24 Changes. *Front Cell Neurosci* **2019**, *13*, 403.

25 39. Klein, J., Phenserine. *Expert Opin Investig Drugs* **2007**, *16* (7), 1087-97.

26 40. Simmons, B. J.; Hoffmann, M.; Champagne, P. A.; Picazo, E.; Yamakawa, K.; Morrill, L. A.; Houk,
27 K. N.; Garg, N. K., Understanding and Interrupting the Fischer Azaindolization Reaction. *J Am Chem Soc*
28 **2017**, *139* (42), 14833-36.

29 41. Tabrez, S.; Damanhour, G. A., Computational and Kinetic Studies of Acetylcholine Esterase
30 Inhibition by Phenserine. *Curr Pharm Des* **2019**, *25* (18), 2108-2112.

31 42. Santillo, M. F.; Liu, Y., A fluorescence assay for measuring acetylcholinesterase activity in rat
32 blood and a human neuroblastoma cell line (SH-SY5Y). *J Pharmacol Toxicol Methods* **2015**, *76*, 15-22.

33 43. Brandt, R. B.; Laux, J. E.; Yates, S. W., Calculation of inhibitor K_i and inhibitor type from the
34 concentration of inhibitor for 50% inhibition for Michaelis-Menten enzymes. *Biochem Med Metab Biol*
35 **1987**, *37* (3), 344-9.

36 44. Airola, M. V.; Shanbhogue, P.; Shamseddine, A. A.; Guja, K. E.; Senkal, C. E.; Maini, R.; Bartke, N.;
37 Wu, B. X.; Obeid, L. M.; Garcia-Diaz, M.; Hannun, Y. A., Structure of human nSMase2 reveals an
38 interdomain allosteric activation mechanism for ceramide generation. *Proc Natl Acad Sci USA* **2017**, *114*
39 (28), E5549-E5558.

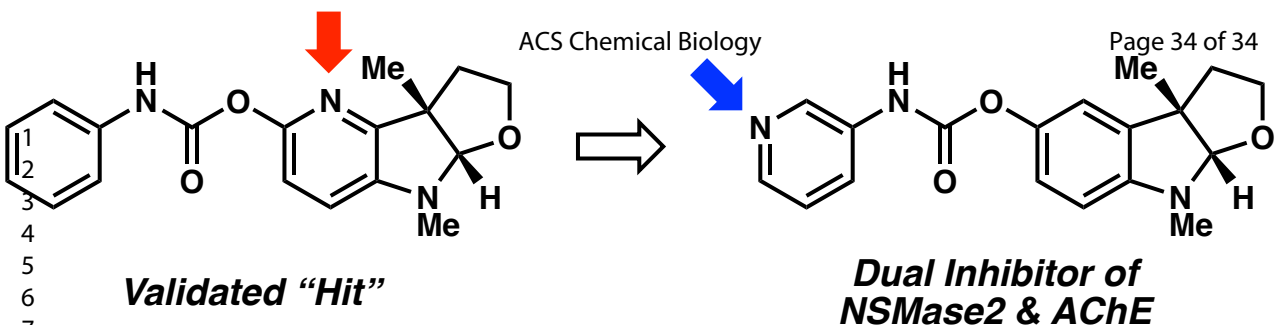
40 45. Park, S. J.; Kim, J. M.; Kim, J.; Hur, J.; Park, S.; Kim, K.; Shin, H.-J.; Chwae, Y.-J., Molecular
41 mechanisms of biogenesis of apoptotic exosome-like vesicles and their roles as damage-associated
42 molecular patterns. *Proc Natl Acad Sci USA* **2018**, *115* (50), E11721-30.

43 46. Zhang, X.-J.; Greenberg, D. S., Acetylcholinesterase involvement in apoptosis. *Front Mol Neurosci*
44 **2012**, *5*, 40.

45 47. Nalivaeva, N. N.; Rybakina, E. G.; Pivanovich, I.; Kozinets, I. A.; Shanin, S. N.; Bartfai, T.,
46 Activation of neutral sphingomyelinase by IL-1 β requires the type 1 interleukin 1 receptor. *Cytokine*
47 **2000**, *12* (3), 229-32.

48 48. Yoshiyama, Y.; Higuchi, M.; Zhang, B.; Huang, S. M.; Iwata, N.; Saido, T. C.; Maeda, J.; Suhara, T.;
49 Trojanowski, J. Q.; Lee, V. M., Synapse loss and microglial activation precede tangles in a P301S
50 tauopathy mouse model. *Neuron* **2007**, *53* (3), 337-51.

- 1
2
3 49. Kitazawa, M.; Cheng, D.; Tsukamoto, M. R.; Koike, M. A.; Wes, P. D.; Vasilevko, V.; Cribbs, D. H.;
4 LaFerla, F. M., Blocking IL-1 signaling rescues cognition, attenuates tau pathology, and restores neuronal
5 beta-catenin pathway function in an Alzheimer's disease model. *J Immunol* **2011**, *187* (12), 6539-49.
- 6 50. Ghosh, S.; Wu, M. D.; Shaftel, S. S.; Kyrkanides, S.; LaFerla, F. M.; Olschowka, J. A.; O'Banion, M.
7 K., Sustained interleukin-1beta overexpression exacerbates tau pathology despite reduced amyloid
8 burden in an Alzheimer's mouse model. *Journal of Neurosci* **2013**, *33* (11), 5053-64.
- 9 51. Dickens, A. M.; Tovar-y-Romo, L. B.; Yoo, S.-W.; Trout, A. L.; Bae, M.; Kanmogne, M.; Megra, B.;
10 Williams, D. W.; Witwer, K. W.; Gacias, M.; Tabatadze, N.; Cole, R. N.; Casaccia, P.; Berman, J. W.;
11 Anthony, D. C.; Haughey, N. J., Astrocyte-shed extracellular vesicles regulate the peripheral leukocyte
12 response to inflammatory brain lesions. *Sci Signal*. **2017**, *10* (473), eaai7696.
- 13 52. Vella, L. J.; Scicluna, B. J.; Cheng, L.; Bawden, E. G.; Masters, C. L.; Ang, C. S.; Williamson, N.;
14 McLean, C.; Barnham, K. J.; Hill, A. F., A rigorous method to enrich for exosomes from brain tissue. *J*
15 *Extracell Vesicles* **2017**, *6* (1), 1348885.
- 16 53. Baietti, M. F.; Zhang, Z.; Mortier, E.; Melchior, A.; Degeest, G.; Geeraerts, A.; Ivarsson, Y.;
17 Depoortere, F.; Coomans, C.; Vermeiren, E.; Zimmermann, P.; David, G., Syndecan-syntenin-ALIX
18 regulates the biogenesis of exosomes. *Nat Cell Biol* **2012**, *14* (7), 677-85.
- 19 54. Liu, X.; Nemeth, D. P.; McKim, D. B.; Zhu, L.; DiSabato, D. J.; Berdysz, O.; Gorantla, G.; Oliver, B.;
20 Witcher, K. G.; Wang, Y.; Negray, C. E.; Vegesna, R. S.; Sheridan, J. F.; Godbout, J. P.; Robson, M. J.;
21 Blakely, R. D.; Popovich, P. G.; Bilbo, S. D.; Quan, N., Cell-Type-Specific Interleukin 1 Receptor 1 Signaling
22 in the Brain Regulates Distinct Neuroimmune Activities. *Immunity* **2019**, *50* (2), 317-333 e6.
- 23 55. Maphis, N.; Xu, G.; Kokiko-Cochran, O. N.; Jiang, S.; Cardona, A.; Ransohoff, R. M.; Lamb, B. T.;
24 Bhaskar, K., Reactive microglia drive tau pathology and contribute to the spreading of pathological tau in
25 the brain. *Brain* **2015**, *138* (Pt 6), 1738-55.
- 26 56. Crotti, A.; Sait, H. R.; McAvoy, K. M.; Estrada, K.; Ergun, A.; Szak, S.; Marsh, G.; Jandreski, L.;
27 Peterson, M.; Reynolds, T. L.; Dalkilic-Liddle, I.; Cameron, A.; Cahir-McFarland, E.; Ransohoff, R. M., BIN1
28 favors the spreading of Tau via extracellular vesicles. *Sci Rep* **2019**, *9* (1), 9477.
- 29 57. Gomez-Ramos, A.; Diaz-Hernandez, M.; Rubio, A.; Diaz-Hernandez, J. I.; Miras-Portugal, M. T.;
30 Avila, J., Characteristics and consequences of muscarinic receptor activation by tau protein. *Eur*
31 *Neuropsychopharmacol* **2009**, *19* (10), 708-17.
- 32 58. Uwada, J.; Yoshiki, H.; Masuoka, T.; Nishio, M.; Muramatsu, I., Intracellular localization of the
33 M1 muscarinic acetylcholine receptor through clathrin-dependent constitutive internalization is
34 mediated by a C-terminal tryptophan-based motif. *J Cell Sci* **2014**, *127* (Pt 14), 3131-40.
- 35 59. Perez, M.; Avila, J.; Hernandez, F., Propagation of Tau via Extracellular Vesicles. *Front Neurosci*
36 **2019**, *13*, 698.
- 37
38
39
40
41
42
43
44
45
46
47
48
49
50
51
52
53
54
55
56
57
58
59
60



New Approach for the Treatment of Alzheimer's Disease

- **Suppresses presynaptic tau-bearing exosome release**
- **Decreases postsynaptic uptake of tau oligomers**
- **Supports cholinergic functions**